Supporting Information

Conformal Shell Amorphization of Nanoporous Ag-Bi for Efficient Formate Generation

Xiangji Zhou,[†] Xianglong Lu,[†] Tianshui Yu,[†] Hailing Wang,[†] Lihua Qian,[*,†] Pengxiang Lei,[‡] Yao Yu,[§] Lin Liu,[§] Shengguo Xia[‖] and Jiakun Fang[‖]

† School of Physics, Huazhong University of Science and Technology, Wuhan 430074, China.
‡ School of Chemistry and Chemical Engineering, Hubei University of Technology, Wuhan 430068, China.
§ School of Materials Science and Engineering, Huazhong University of Science and Technology, Wuhan, 430074, China.
‖ State Key Lab of Advanced Electromagnetic Engineering and Technology, School of Electrical and Electronic Engineering, Huazhong University of Science and Technology, Wuhan 430074, China.

Corresponding Author
***L. Qian. E-mail: lhqian@hust.edu.cn**

Contents of supporting information:

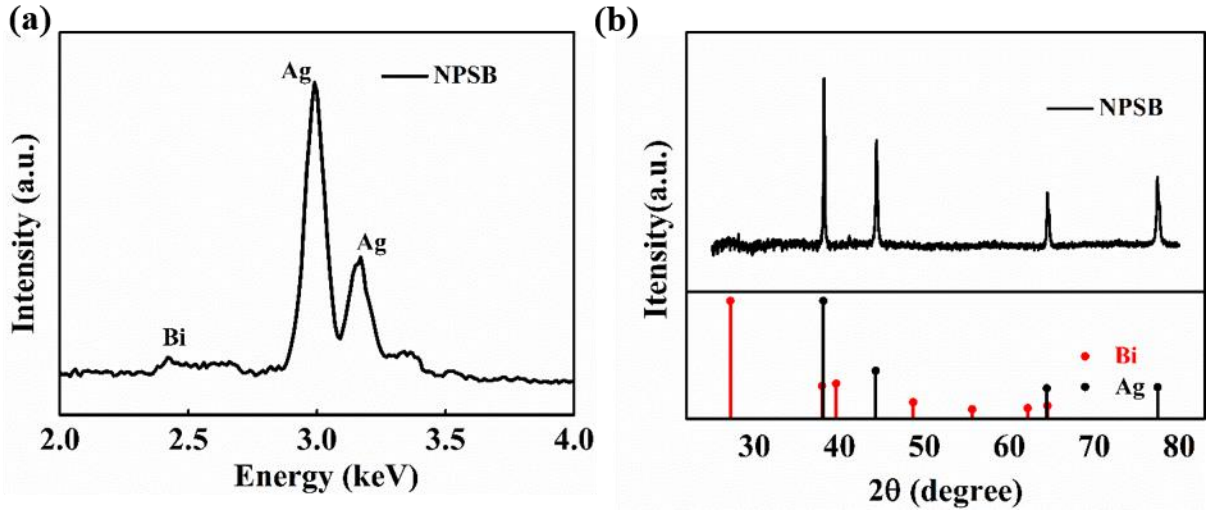

Figure S1. (a) The EDS pattern of the NPSB indicates atomic concentration of Bi element as 2.27 atom %. (b) The XRD pattern of the NPSB shows four sharp diffraction peaks corresponding to Ag polycrystal. No signal can be detected from Bi crystal, implying the formation of Ag-Bi solid solution.

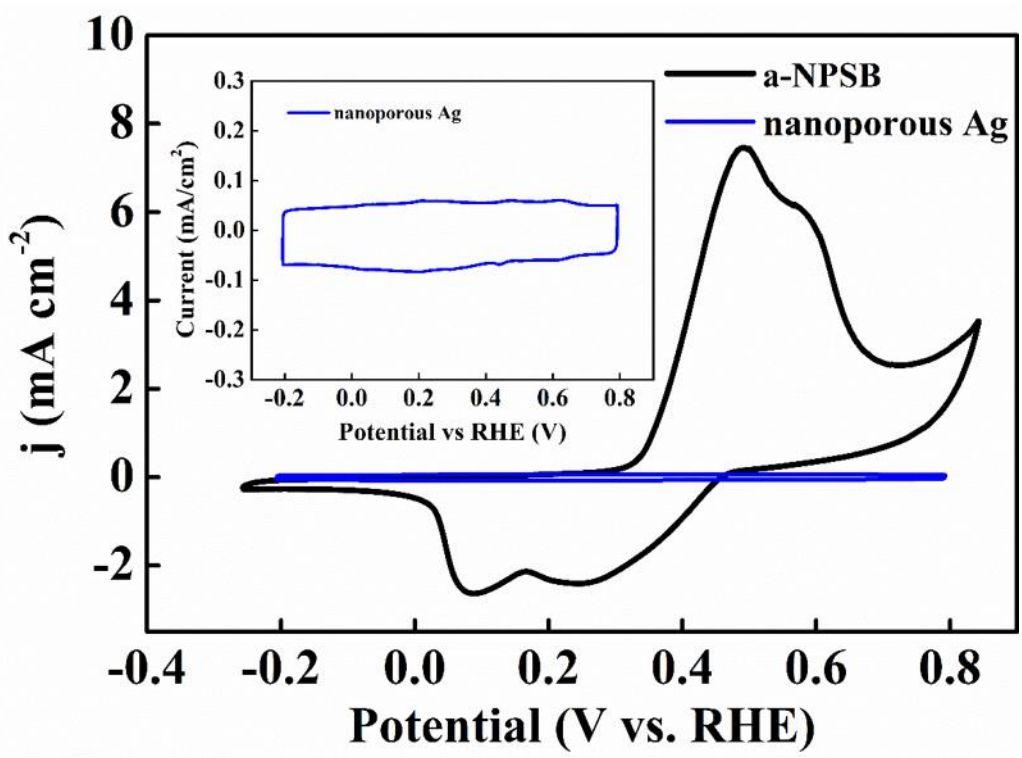

Figure S2. The CV curves of the a-NPSB and nanoporous Ag. The electrochemical measurement is conducted in CO_2 saturated 0.1 M $KHCO_3$ electrolyte with scan rate of 5 mV/s. The redox peaks of the a-NPSB correspond to the dissolution of amorphous Bi_2O_3 and Bi deposition on the a-NPSB. The redox of Ag atoms does not get involved in this potential range.

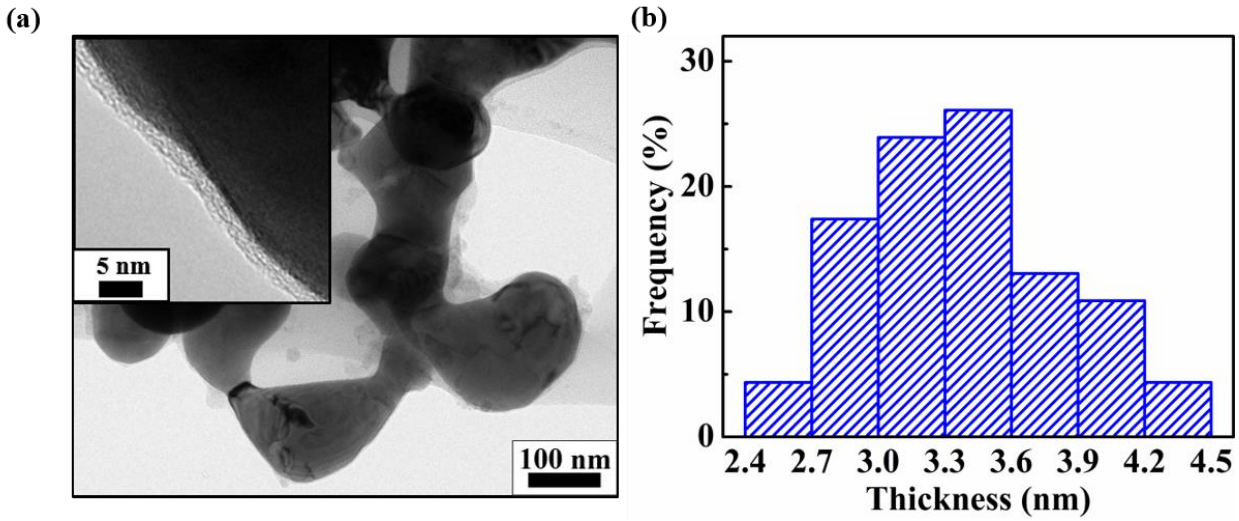

Figure S3. (a) TEM and HRTEM images of the a-NPSB. (b) Statistical distribution on the thickness of amorphous Bi_2O_3 layer based on the morphology.

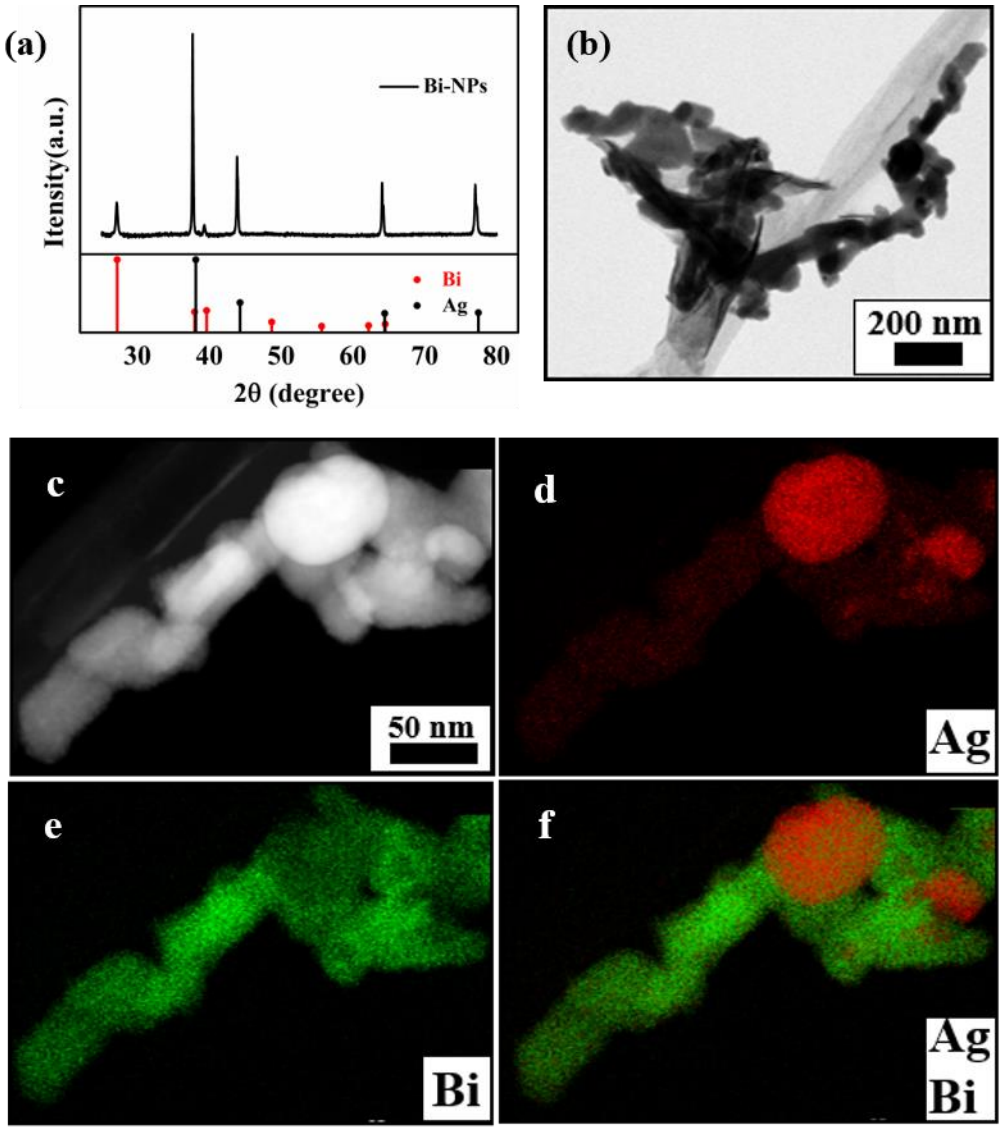

Figure S4. (a) XRD pattern, (b) TEM image, (c) STEM image and (d-f) element mapping images of the Bi-NPs with tens of nm.

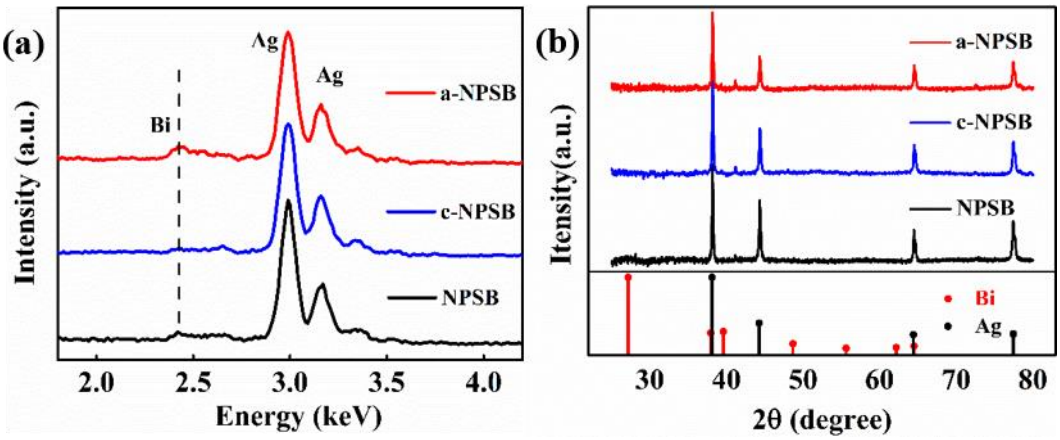

Figure S5. (a) The EDS and (b) XRD patterns of the NPSB, the c-NPSB and the c-NPSB. Bi signal is weak, and Ag signals from different samples show the nearly identical profile. XRD patterns of nanoporous Ag and the a-NPSB show one isolate Ag phase, implying that Bi elements are diluted into Ag lattice. The diffraction peak at 43° is the low level of residual Ag_2Al that cannot be dissolved by chemical dealloying.

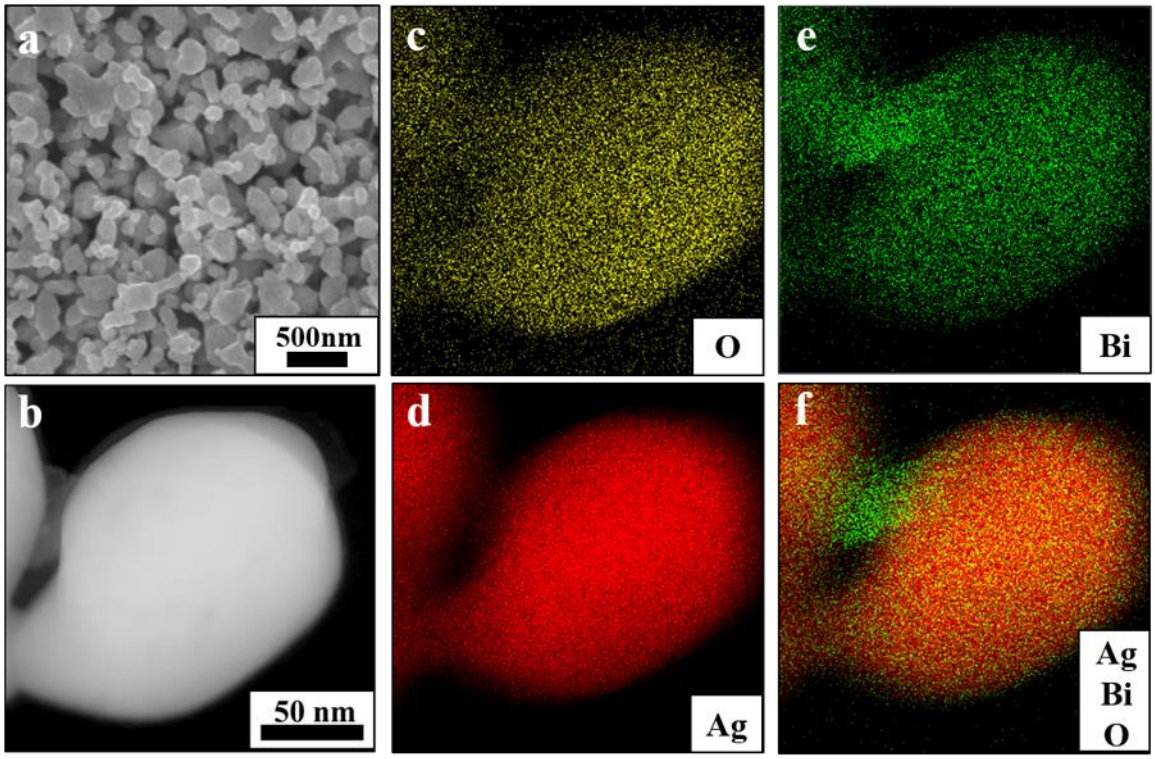

Figure S6. The morphology and element distribution of the ligaments in the c-NPSB. (a-b) SEM and STEM images of the c-NPSB exhibit the similar morphology with the a-NPSB. But no amorphous shell on the c-NPSB is observed on the surface of most ligaments. (c-f) Element mapping of Ag, Bi, O verifies that most of amorphous Bi_2O_3 shells are dissolved when the a-NPSB is subjected to multiple CV stripping. Thus, some Bi elements are detected from the electrolytes after CV stripping by means of the ICP-OES.

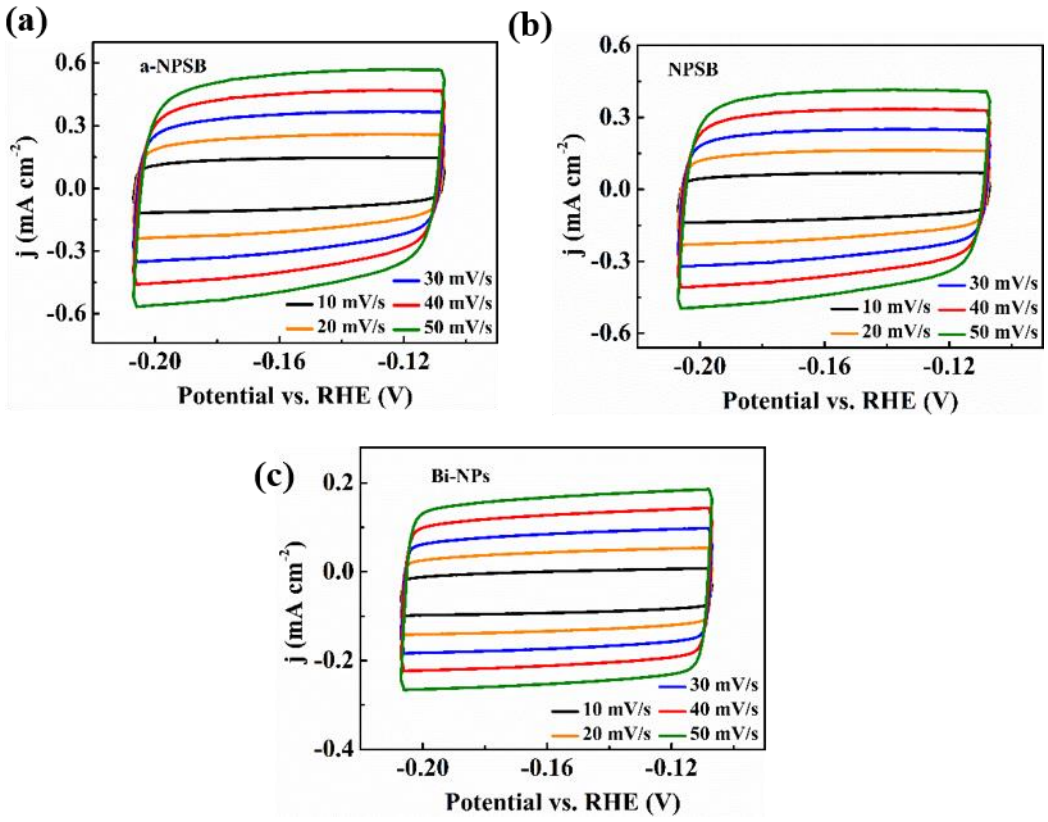

Figure S7. Cyclic voltammograms of (a) a-NPSB, (b) NPSB and (c) Bi-NPs with different scan rates.

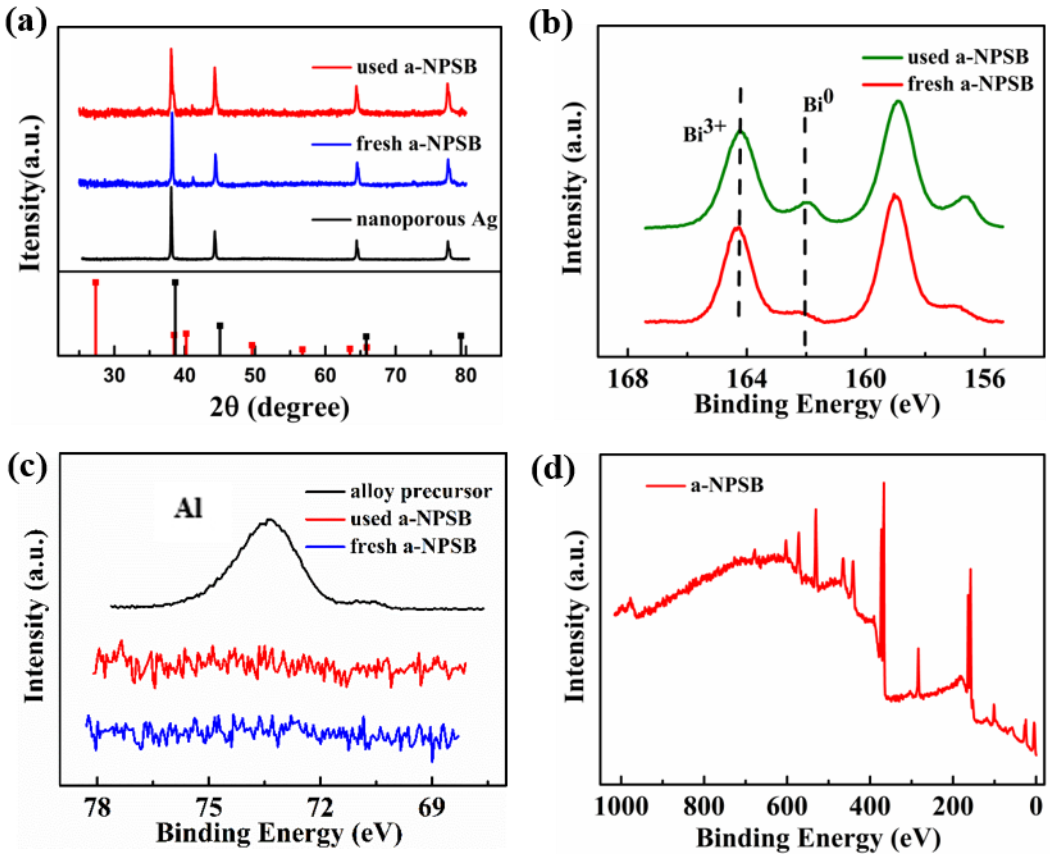

Figure S8. (a) XRD patterns of the used a-NPSB, fresh a-NPSB and nanoporous Ag. XPS patterns of (b) Bi and (c) Al elements on fresh a-NPSB and the a-NPSB after 18 hours electrochemical catalytic reaction. The Al signal is absent in the high resolution XPS, implying that the residual Ag_2Al locates at the inner skeletons rather than ligament surface. (d) XPS surveyed spectrum of the a-NPSB.

Table S1 The ICP-OES analysis shows the Bi concentration in the NPSB, and the real concentration of NPSB detected by ICP-OES approaches to the expected concentration. The content of Bi in NPSB calculated based on the real concentration is 2.18%. The real concentration of Bi element in electrolyte is close to the expected concentration, demonstrating the dissolution of the amorphous Bi_2O_3 shell.

Electrode or electrolyte	Expected concentration (ppm)	Real concentration (ppm)
NPSB	7.663	6.9035
Electrolyte	0.0223	0.0294

Table S2 CO_2ER catalytic properties of various Bi derived catalysts.

Electrocatalyst	Electrolyte	Potential	Current density	FE	Stability test	Reference
Nanoporous Ag@ Bi_2O_3	0.1 M $KHCO_3$	-1.15 V vs. RHE	21.2 mA cm^{-2}	88.4%	18 h	This work
Bi_2O_3NSs@MCCM	0.1 M $KHCO_3$	-1.356 V vs. RHE	17.7 mA cm^{-2}	~90%	12 h	1
3D fractal structures of Bi_2O_3	0.1 M $KHCO_3$	-1.2 V vs. RHE	24 mA cm^{-2}	87%	6 h	2
Nanotube-derived Bi	0.5 M $KHCO_3$	-0.82 V vs. RHE	36 mA cm^{-2}	~98%	48 h	3
Bi_2O_3 with enhanced Bi-O	0.5 M $KHCO_3$	-0.9 V vs. RHE	~8 mA cm^{-2}	91%	24 h	4
Bi nanoparticles/ Bi_2O_3 nanosheet	0.5 M $NaHCO_3$	-0.86 V vs. RHE	10 mA cm^{-2}	>90%	24 h	5
BiOx/C	0.5 M $NaHCO_3$ and 0.5 M $NaClO_4$	-1.75 V vs. Ag/AgCl	16.1 mA cm^{-2}	93.4%	3 h	6
Bi nanosheet	0.5 M $NaHCO_3$	-1.5 V vs. SCE	14 mA cm^{-2}	~95%	10 h	7
Defect-rich Bi	0.5 M $NaHCO_3$	-0.75 V vs. RHE	5.0 mA cm^{-2}	84%	24 h	8

(1) Liu, S.; Lu, X.; Xiao, J.; Wang, X.; Lou, X. Bi_2O_3 Nanosheets Grown on Multi-Channel Carbon Matrix to Catalyze Efficient CO_2 Electroreduction to HCOOH. *Angew. Chem. Int. Ed.* **2019**, *58*, 13828-13833.
(2) Tran-Phu, T.; Daiyan, R.; Fusco, Z.; Ma, Z.; Amal, R.; Tricoli, A. Nanostructured β-Bi_2O_3 Fractals on Carbon Fibers for Highly Selective CO_2 Electroreduction to Formate. *Adv. Funct. Mate.* **2019**, *30*, 1906478.
(3) Gong, Q.; Ding, P.; Xu, M.; Zhu, X.; Wang, M.; Deng, J.; Ma, Q.; Han, N.; Zhu, Y.; Lu, J.; Feng, Z.; Li, Y.; Zhou, W.; Li, Y. Structural Defects on Converted Bismuth Oxide Nanotubes Enable Highly Active Electrocatalysis of Carbon Dioxide Reduction. *Nat. Commun.* **2019**, *10*, 2807.
(4) Deng, P.; Wang, H.; Qi, R.; Zhu, J.; Chen, S.; Yang, F.; Zhou, L.; Qi, K.; Liu, H.; Xia, B. Bismuth Oxides with Enhanced Bismuth-Oxygen Structure for Efficient Electrochemical Reduction of Carbon Dioxide to Formate. *ACS Catal.* **2020**, *10*, 743−750.
(5) Li, L.; Ma, D.; Qi, F.; Chen, W.; Huang, S. Bi Nanoparticles/Bi_2O_3 Nanosheets with Abundant Grain Boundaries for Efficient Electrocatalytic CO_2 Reduction. *Electrochimica Acta* **2019**, *298*, 580-586.
(6) Lee, C. W.; Hong, J. S.; Yang, K. D.; Jin, K.; Lee, J. H.; Ahn, H.-Y.; Seo, H.; Sung, N.-E.; Nam, K. T. Selective Electrochemical Production of Formate from Carbon Dioxide with Bismuth-Based Catalysts in an Aqueous Electrolyte. *ACS Catal.* **2018**, *8*, 931−937.
(7) Han, N.; Wang, Y.; Yang, H.; Deng, J.; Wu, J.; Li, Y.; Li, Y. Ultrathin Bismuth Nanosheets from in Situ Topotactic Transformation for Selective Electrocatalytic CO_2 Reduction to Formate. *Nat. Commun.* **2018**, *9*, 1320.
(8) Zhang, Y.; Li, F.; Zhang, X.; Williams, T.; Easton, C. D.; Bond, A. M.; Zhang, J. Electrochemical Reduction of CO_2 on Defect-rich Bi Derived from Bi_2S_3 with Enhanced Formate Selectivity. *J. Mater. Chem. A* **2018**, *6*, 4714-4720.